Research Article

Journal of Environmental Nanotechnology

Parametric Study on the Tribological Response of WAAM-deposited Aluminium 8090/Nano-TiC Metal Matrix Composites

B. Silambarasan[1*], A. Backia Abinaya[2], G. Karthikeyan[3], S. N. Dinesh[4] and U. Vivek[5]

[1]Department of Mechanical Engineering, Sir Issac Newton College of Engineering and Technology, Nagapattinam, TN, India
[2]Department of Electronics and Communication Engineering, St. Joseph's College of Engineering and Technology, Thanjavur, TN, India
[3]Department of Mechanical Engineering, University College of Engineering, BIT Campus, Tiruchirappalli, TN, India
[4]Department of Mechanical Engineering, KPR Institute of Engineering and Technology, Coimbatore, TN, India
[5]Department of Mechanical Engineering, K. S. Rangasamy College of Technology, KSR Kalvi Nagar, Tiruchengode, TN, India
Received: 26.01.2026 Accepted: 15.02.2026 Published: 30.03.2026
*balasimbu05@gmail.com

ABSTRACT

Wire Arc Additive Manufacturing (WAAM) offers a promising route for fabricating large-scale aluminium components. However, the tribological performance of WAAM-processed aluminium alloys remains a critical limitation for wear-sensitive applications. In this study, Aluminium 8090 alloy reinforced with 1 wt.% nano-sized titanium carbide (TiC) was fabricated using the WAAM process, and its tribological behaviour under dry sliding conditions was systematically investigated. A Taguchi L27 orthogonal array was employed to evaluate the influence of the applied load, sliding velocity, and sliding distance on the wear rate and coefficient of friction (COF). Statistical tools, including signal-to-noise ratio analysis, analysis of variance, contour plots, and regression modelling were used to identify the dominant wear-controlling parameters and optimize the operating conditions. The results revealed that sliding velocity was the most influential parameter affecting both wear rate and COF, followed by applied load, while sliding distance exhibited a comparatively minor effect. The incorporation of nano-TiC significantly enhanced the load-bearing capacity, resulting in improved hardness and reduced wear under moderate operating conditions. The SEM analysis of the worn surfaces indicated a transition from mild adhesive wear at lower loads to abrasive and fatigue-dominated wear at higher loads, corroborating the experimental and statistical findings. The developed regression models demonstrated good predictive capability within the investigated parameter range. This study established clear structure–property–performance correlations and demonstrated the potential of WAAM-fabricated Al8090–nano-TiC composites for wear-critical engineering applications.

Keywords: Wire arc additive manufacturing; Aluminium 8090 alloy; Nano-TiC metal matrix composite; Tribological behavior; Wear rate.

1. INTRODUCTION

Additive manufacturing (AM) has emerged as a transformative manufacturing architype for producing complex metallic components with high material utilization, geometric freedom, and reduced postprocessing requirements compared to conventional subtractive routes (Sathish *et al.* 2022). Among the various AM techniques, Wire Arc Additive Manufacturing (WAAM) has gained particular attention for aluminium alloys due to its high deposition rate, scalability, cost-effectiveness, and suitability for large structural components (Ingarao and Priarone, 2020; Klein *et al.* 2021). Unlike powder-based AM processes, WAAM employs wire feedstock, which minimizes material loss, reduces contamination risks, and offers superior process efficiency, making it especially attractive for aluminium-based systems in the aerospace and transportation sectors. However, the thermal cycling inherent to the WAAM process often results in layer-wise anisotropy, coarse columnar grains, residual stresses, and porosity, which can adversely affect the mechanical integrity and tribological performance (Çam, 2022; Rathod, 2025). Consequently, enhancing the wear resistance and frictional stability of WAAM-fabricated aluminium alloys remains a critical challenge for their use in wear-critical applications.

Aluminium 8090, a lithium-containing aluminium alloy, is widely utilized in aerospace structures owing to its low density, high specific strength, and excellent fatigue resistance (Li *et al.* 2023; Nouri *et al.* 2019). Despite these advantages, Al8090 exhibits inherently poor tribological performance under dry sliding conditions, primarily because of its relatively low hardness and susceptibility to adhesive and abrasive wear. This limitation restricts its application to components subjected to sustained frictional contact. Reinforcement of Al8090 with

ceramic particulates has been widely explored as an effective strategy to improve its hardness, load-bearing capability, and wear resistance. Previous studies have demonstrated that reinforcements such as SiC (Wu and Pei, 2024) B_4C (Karthe *et al.* 2023), TiB_2 (Kaviyarasan *et al.* 2022), and graphite (Yekinni *et al.* 2020) can significantly enhance the tribological response of Al8090-based composites. However, most of these investigations have focused on conventionally fabricated composites, and the translation of these improvements to WAAM-processed Al8090 systems remains insufficiently understood.

Among the available ceramic reinforcements, titanium carbide (TiC) is particularly attractive because of its high hardness, excellent thermal stability, low density, and strong interfacial compatibility with aluminium matrices (Ao *et al*. 2021; Kar and Surekha, 2019; Dwivedi *et al.* 2023). The primary motivation for reinforcing Al8090 with TiC in a WAAM environment is twofold: first, TiC acts as a thermally stable load-bearing phase capable of resisting severe contact stresses during sliding; second, TiC particles can restrict grain growth during repeated thermal cycling, thereby refining the microstructure formed during the layer-by-layer deposition (Agrawal *et al.* 2023). Compared to micro-sized reinforcements, nano-sized TiC particles offer a substantially higher surface area-to-volume ratio, which promotes improved interfacial bonding, more efficient load transfer, and effective obstruction of dislocation motion in the matrix (Pan *et al.* 2020). Collectively, these mechanisms contribute to enhanced hardness, reduced plastic deformation, and superior wear resistance (Yu *et al.* 2023). In contrast, micro-sized reinforcements are more prone to particle pull-out, stress concentration, and non-uniform distribution, which can degrade their tribological performance under high loads.

The layer-by-layer nature of the WAAM process further amplifies the importance of the reinforcement selection. During WAAM deposition, successive thermal cycles influence the solidification behavior, grain morphology, and defect formation. In unreinforced aluminium alloys, this often leads to coarse columnar grains aligned along the build direction and localized porosity. The incorporation of uniformly dispersed nano-TiC particles can significantly modify this behavior by acting as heterogeneous nucleation sites, disrupting epitaxial grain growth, and promoting a refined and equiaxed grain structure (Cabeza *et al.* 2017). Moreover, the uniform dispersion of TiC enhanced the load-bearing capacity of the composite by ensuring a homogeneous stress distribution across the sliding interface. Well-dispersed nanoparticles prevent localized stress accumulation, reduce direct metal-to-metal contact, and facilitate the formation of a stable tribolayer, thereby lowering the wear rate and stabilizing the coefficient of friction (COF) (Le *et al.* 2025).

The tribological response of aluminium matrix composites is highly sensitive to operational parameters such as the applied load, sliding velocity and sliding distance. Variations in these parameters influence the contact stress, interfacial temperature, debris formation, and tribo-oxide stability. To systematically evaluate these effects, statistical optimization tools such as Taguchi design, analysis of variance (ANOVA) (Arunkumar *et al*. 2020), response surface methodology (Ashok and Devaraju, 2021) and grey relational analysis (Shivakumar and Panchangam, 2024) have been extensively employed in conventional modular multilevel converter systems. These approaches enable the quantitative assessment of parameter significance, predictive modeling, and multi-objective optimization with reduced experimental effort. However, the application of such parametric optimization frameworks to WAAM-deposited Al8090 composites reinforced with nano-sized TiC remains limited, particularly with respect to establishing clear structure–property–tribology relationships.

Based on the identified research gaps, this study systematically investigated the tribological behavior of WAAM-fabricated Al8090/nano-TiC metal matrix composites under dry sliding conditions. This study emphasizes (i) the role of nano-TiC reinforcement in enhancing the load-bearing capacity and wear resistance, (ii) the influence of WAAM-induced microstructural features on tribological performance, and (iii) the statistical optimization of key wear parameters using a design-of-experiments approach. The outcomes of this study are expected to provide critical insights into the design and optimization of WAAM-processed aluminium-based composites for advanced aerospace and automotive applications.

2. MATERIALS AND METHODS

2.1 Materials

The material system investigated in this study consists of Aluminium 8090 alloy reinforced with 1 wt.% nano-sized titanium carbide particles, fabricated using the WAAM process. Aluminium 8090 (Al–Li alloy) was selected due to its low density, high specific strength, and extensive application in aerospace structures; however, its relatively low hardness and poor resistance to adhesive and abrasive wear under dry sliding conditions limit its use in tribological components (Azo Network report, 2013).

The selection of 1 wt.% TiC reinforcement was based on a balanced consideration of tribological performance enhancement, processability in WAAM,

and microstructural stability. At low reinforcement levels (≤1 wt.%), nano-TiC particles can be uniformly dispersed within the aluminium matrix, providing effective load-bearing capability and grain refinement without significantly increasing melt viscosity or causing particle agglomeration. Higher reinforcement contents are known to promote particle clustering, poor wetting, increased porosity, and arc instability during wire-based additive manufacturing, adversely affecting deposit integrity and surface quality. Therefore, 1 wt.% TiC represents an optimum reinforcement level that enhances wear resistance while maintaining stable wire feeding, melt pool fluidity, and defect-free deposition.

From a microstructural perspective, the nano-TiC particles at 1 wt.% act as heterogeneous nucleation sites during solidification, restricting grain growth induced by the repeated thermal cycling inherent to the WAAM process. This resulted in a refined microstructure with improved interfacial bonding and reduced anisotropy. Tribologically, the selected reinforcement fraction provides a sufficient population of hard ceramic particles to share the applied load, suppress plastic deformation, and minimize direct metal-to-metal contact, thereby reducing the wear rate and stabilizing the COF under dry sliding conditions (Du *et al.* 2023).

A nano-treated Al8090–1 wt.% TiC filler wire with a diameter of 1.2 mm was used as the feedstock material to ensure consistent reinforcement distribution throughout the deposited structure. The chemical composition of the filler wire is listed in Table 1. A 35-mm thick Al8090 alloy plate was used as the substrate material to ensure metallurgical compatibility and minimize the thermal expansion mismatch during deposition.

Table 1. Chemical composition of Al8090−1 wt.% TiC filler wire (wt.%)

Material	Li	Cu	Mg	Zn	Mn	Si	Fe	Ti	Al
Al8090–TiC	2.3	1.3	0.9	0.8	0.3	0.1	0.15	0.1	93.95

2.2 Method of Fabrication

The Al8090–nano-TiC composite was fabricated using a robot-assisted WAAM setup comprising a cold metal transfer welding power source (Fronius TPS400i, Austria) integrated with a six-axis robotic manipulator (YASKAWA GP12/AR1440). Prior to deposition, the substrate surface was mechanically ground, cleaned, and degreased to remove oxide layers and surface contaminants, thereby ensuring a strong metallurgical bond between the substrate and deposited layers.

The deposition was carried out using optimized process parameters with a wire feed speed of 8 m/min and a torch travel speed of 150 mm/min. An arc length correction of –5% was applied to stabilize the molten pool, during deposition. High-purity argon was used as the shielding gas to prevent the oxidation of the molten pool. Using a multilayer, single-pass deposition strategy, a wall structure with approximate dimensions of 160 mm (length), 25 mm (width), and 35 mm (height) was fabricated by depositing 18 layers, each with an average thickness of approximately 1.94 mm (Fig. 1).

2.3 Experimental Details

The extracted specimens were machined to the required dimensions based on the specific characterization techniques. For tribological testing, pin specimens with a diameter of 10 mm and length of 30 mm were prepared in accordance with the ASTM G99 standards using wire electrical discharge machining, as shown in Fig. 2. All specimens were ultrasonically cleaned with acetone prior to testing to eliminate surface contaminants. The experimental investigation focused on evaluating the microstructural integrity, hardness, and tribological behavior of WAAM-fabricated Al8090–TiC composites. A systematic design of experiments approach was adopted to study the influence of the applied load, sliding velocity, and sliding distance on the wear rate and COF. All tests were conducted under dry sliding conditions at an ambient temperature.

2.4 Testing of Al8090−TiC WAAM Composites

2.4.1 Energy Dispersive Spectroscopy Analysis

Energy Dispersive Spectroscopy (Make: Bruker X-Flash) coupled with Scanning Electron Microscopy (SEM) (Make: Zeiss EVO 18) was employed to confirm the presence and distribution of TiC particles within the WAAM-deposited Al8090 matrix. Polished cross-sectional specimens were examined to assess the elemental homogeneity and reinforcement dispersion.

2.4.2 Hardness Measurement

Microhardness measurements were conducted to evaluate the influence of the nano-TiC reinforcement and WAAM processing on the mechanical response of the composite. A Vickers microhardness tester was used

with a standard load and dwell time (according to ASTM E384). Multiple indentations were taken across different layers of the deposited structure to account for potential layer-wise variations caused by thermal cycling. The average hardness was reported to ensure statistical reliability.

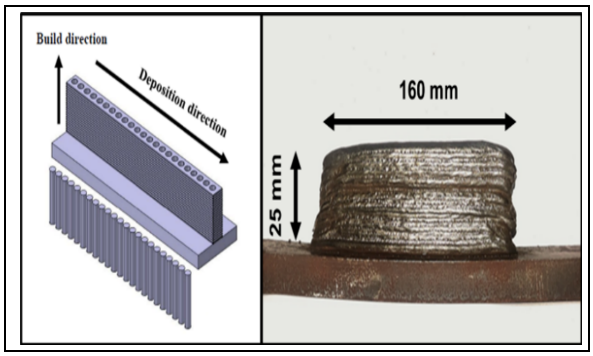


Fig. 1: WAAM-fabricated Al8090–nano-TiC composite using a multilayer deposition

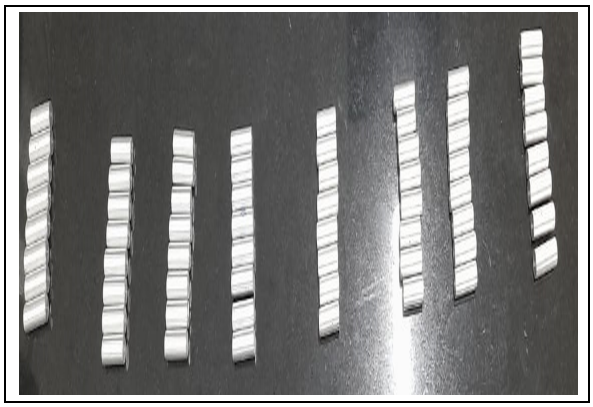


Fig. 2: Cylindrical specimens for mechanical and tribological testing

2.4.3 Wear Testing of WAAM-Fabricated Al8090–TiC Composite

Dry sliding wear tests were performed using a pin-on-disc tribometer (Make: DUCOM TR-20LE) in accordance with ASTM G99, as shown in Fig. 3. The Al8090–TiC composite pins were tested against a hardened EN-8 steel disc. The experiments were conducted under varying applied loads (10, 20, and 30 N), sliding velocities (1, 2, and 3 m/s), and sliding distances (500, 1000, and 1500 m), as listed in Table 2. During testing, the wear displacement and frictional force were continuously recorded using an integrated data-acquisition system. The wear rate (mm^3/m) was calculated based on the volumetric material loss, while the COF was obtained from the ratio of the frictional force to the applied load. Each experiment was conducted under identical environmental conditions to ensure its repeatability. The post-wear surface morphology was analyzed using SEM to identify the dominant wear mechanisms.

To systematically evaluate the influence of tribological parameters and minimize experimental variability, a Taguchi design of experiments (DOE) approach was employed. An L27 (3^3) orthogonal array was selected to study the combined effects of the applied load, sliding velocity, and sliding distance, each of which was varied at three levels. The L27 array allows for the independent assessment of the main factor effects while reducing the experimental effort compared to full factorial designs, thereby ensuring statistical robustness and reproducibility. The selected control factors and their respective levels were chosen based on preliminary trials to represent realistic service conditions for aluminium-based composites during dry sliding wear. The experimental layout of the L27 orthogonal array with only input parameters is presented in Table 3.



Fig. 3: Pin-on-disc tribometer used for wear testing

Table 2. Experimental control parameters and levels

Control Parameter	Unit	Level 1	Level 2	Level 3
Applied Load	N	10	20	30
Sliding Velocity	m/s	1	2	3
Sliding Distance	m	500	1000	1500

3. RESULTS AND DISCUSSIONS

3.1 Energy Dispersive Spectroscopy (EDS) Analysis

The energy-dispersive spectroscopy spectrum of the WAAM-fabricated Al8090–nano-TiC composite, presented in Fig. 4, confirms the successful incorporation of nano-TiC reinforcement within the aluminium matrix and the retention of the nominal alloying elements during the WAAM process. Al was the dominant element, with a measured content of approximately 93.6 wt. %, which is consistent with the expected composition of Aluminium 8090 alloys. The presence of titanium (0.9 wt.%) and carbon (0.8 wt.%) provides direct evidence of TiC reinforcement, indicating that the carbide particles remain chemically

stable and do not undergo significant dissolution or reaction during the high-thermal-input WAAM deposition.

Table 3. L27 Taguchi orthogonal array showing input parameters for wear testing

Experiment No.	Applied Load (N)	Sliding Velocity (m/s)	Sliding Distance (m)
1	10	1	500
2	10	1	1000
3	10	1	1500
4	10	2	500
5	10	2	1000
6	10	2	1500
7	10	3	500
8	10	3	1000
9	10	3	1500
10	20	1	500
11	20	1	1000
12	20	1	1500
13	20	2	500
14	20	2	1000
15	20	2	1500
16	20	3	500
17	20	3	1000
18	20	3	1500
19	30	1	500
20	30	1	1000
21	30	1	1500
22	30	2	500
23	30	2	1000
24	30	2	1500
25	30	3	500
26	30	3	1000
27	30	3	1500

Minor alloying elements, such as Cu (1.2 wt.%), Mg (0.9 wt.%), Zn (0.7 wt.%), Mn (0.3 wt.%), Fe (0.15 wt.%), and Si (0.15 wt.%) were also detected, confirming compositional consistency between the deposited material and the filler wire. The absence of extraneous or contaminant elements suggests effective shielding and controlled processing conditions during the WAAM. Slight deviations between the EDS-measured values and the nominal composition are expected because of the surface-sensitive nature of EDS and the localized sampling area.

The uniform detection of the Ti and C peaks across the spectrum further indicates the homogeneous dispersion of the nano-TiC particles, which is critical for improving the load-bearing capacity and wear resistance. Well-distributed TiC particles act as effective obstacles to dislocation motion and suppress localized plastic deformation during sliding, thereby enhancing the tribological performance. Moreover, the chemical stability of TiC under repeated thermal cycling confirms its suitability as a reinforcement phase for WAAM-processed aluminium alloys.

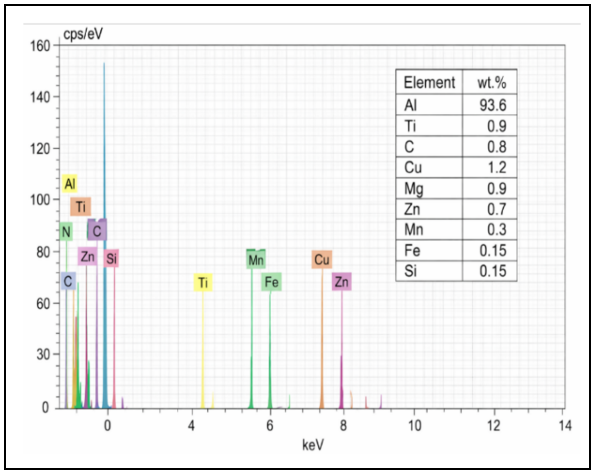


Fig. 4: Elemental analysis of Al8090-TiC composite

3.2 Hardness Analysis

The hardness of the WAAM-fabricated Al8090–nano-TiC composite was evaluated to understand the contribution of the nanoscale reinforcement and WAAM-induced microstructural evolution to the mechanical response of the material. Based on trends reported in the literature for WAAM-fabricated aluminium matrix composites reinforced with TiC and similar ceramic nanoparticles, the composite exhibited an average Vickers microhardness of approximately 128 ± 6 HV, which is substantially higher than that of unreinforced WAAM-processed Al8090 alloys (typically 95–105 HV). The relatively low standard deviation indicates good uniformity of hardness across the deposited layers.

The enhancement in hardness is primarily attributed to the uniform dispersion of the nano-TiC particles within the aluminium matrix, which directly improves the load-bearing capacity of the composite. Uniformly distributed TiC particles act as effective load-sharing constituents, enabling the externally applied load to be transferred from the softer Al matrix to the harder ceramic phase. This homogeneous stress distribution prevents localized stress concentrations and suppresses premature plastic deformation under indentation or sliding contact. In contrast, non-uniform or agglomerated reinforcements can create weak zones that reduce the effective load-bearing efficiency. At the microstructural level, nano-TiC particles impede dislocation motion through Orowan strengthening and particle–matrix interfacial constraints, thereby increasing the resistance to plastic flow (Wang *et al.* 2025). The high hardness and elastic modulus of TiC restricted the penetration of the indenter into the Al matrix, resulting in higher measured hardness values

(Yu *et al.* 2023). Moreover, the nanoscale size of TiC provides a large interfacial area, improving the load transfer efficiency compared to micro-sized reinforcements, which are more prone to particle cracking or pull-out under stress (Chen *et al.* 2023).

The WAAM process further influences the hardness and load-bearing behavior through repeated thermal cycling. While unreinforced WAAM aluminium alloys often exhibit coarse columnar grains and anisotropy, the presence of uniformly dispersed nano-TiC particles suppresses excessive grain growth by acting as heterogeneous nucleation sites during solidification. This grain refinement enhances the hardness *via* the Hall–Petch mechanism and contributes to improved resistance against localized deformation (Zheng *et al.* 2022). Consequently, the composite can sustain higher contact stresses without undergoing severe plastic deformation (Wang *et al.* 2024). The improved load-bearing capacity, as reflected by the increased hardness, directly correlates with the tribological performance of the composite. A harder surface reduces the real area of contact during sliding, limits asperity penetration, and delays the onset of severe-wear mechanisms (Zheng *et al.* 2022). Consequently, the uniform dispersion of nano-TiC not only enhanced the hardness but also provided a strong microstructural foundation for the reduced wear rates and stabilized coefficient of friction observed in the tribological analysis (Qiang *et al.* 2024).

3.3Tribological Analysis

The tribological performance of the WAAM-fabricated Al8090–nano-TiC composite was systematically evaluated using a Taguchi L27 experimental design to quantify the influence of the applied load, sliding velocity, and sliding distance on the wear rate and COF. The experimental results are presented in Table 4. The combined interpretation of the main effects plots, signal-to-noise (S/N) ratio analysis, and ANOVA provides a comprehensive understanding of the dominant wear-controlling mechanisms and frictional behavior under dry sliding conditions.

3.3.1 Effect of Process Parameters on Wear Rate

The main effects plot for the mean wear rate (Fig. 5a) reveals a pronounced increase in wear with increasing applied load and sliding velocity, whereas the sliding distance exhibits a comparatively mild influence. As the applied load increased from 10 N to 30 N, the mean wear rate increased significantly owing to the elevated contact stresses, which intensified the plastic deformation and micro-ploughing of the aluminium matrix. This trend was statistically validated by ANOVA results, where the applied load contributed a significant portion of the total variance ($F = 11.03$, $p = 0.001$), as listed in Table 5.

Table 4. Experimental results of wear rate and coefficient of friction

Experiment No.	Applied Load (N)	Sliding Velocity (m/s)	Sliding Distance (m)	Wear Rate (mm^3/m)	COF
1	10	1	500	0.000065	0.22
2	10	1	1000	0.000087	0.201
3	10	1	1500	0.000099	0.179
4	10	2	500	0.000435	0.175
5	10	2	1000	0.000282	0.204
6	10	2	1500	0.000253	0.211
7	10	3	500	0.000035	0.3
8	10	3	1000	0.000767	0.382
9	10	3	1500	0.000902	0.42
10	20	1	500	0.003146	0.338
11	20	1	1000	0.002405	0.363
12	20	1	1500	0.002202	0.311
13	20	2	500	0.0012	0.18
14	20	2	1000	0.001008	0.188
15	20	2	1500	0.001875	0.326
16	20	3	500	0.010329	0.355
17	20	3	1000	0.011791	0.387
18	20	3	1500	0.012205	0.376
19	30	1	500	0.0021	0.195
20	30	1	1000	0.001978	0.21
21	30	1	1500	0.001959	0.182
22	30	2	500	0.002142	0.076
23	30	2	1000	0.001988	0.134
24	30	2	1500	0.006058	0.192
25	30	3	500	0.010413	0.337
26	30	3	1000	0.016608	0.34
27	30	3	1500	0.015025	0.314

The sliding velocity exerted an even stronger influence on the wear behavior, as evidenced by the steep slope in the main effects plot and the highest F-value (17.47, $p = 0.000$). At low velocities, the wear remained relatively low owing to stable contact and limited thermal softening. However, at higher sliding velocities, frictional heating becomes dominant, leading to the softening of the aluminium matrix and destabilization of protective tribo-oxide layers. Under these conditions, the nano-TiC particles may act as third-body abrasives once detached, accelerating the material removal. In contrast, the sliding distance showed minimal statistical significance ($F = 0.39$, $p = 0.085$), indicating that within the studied range, wear is governed more by instantaneous contact conditions than by cumulative sliding exposure. This suggests that the presence of the nano-TiC reinforcement and tribolayer formation effectively suppressed progressive wear during extended sliding.

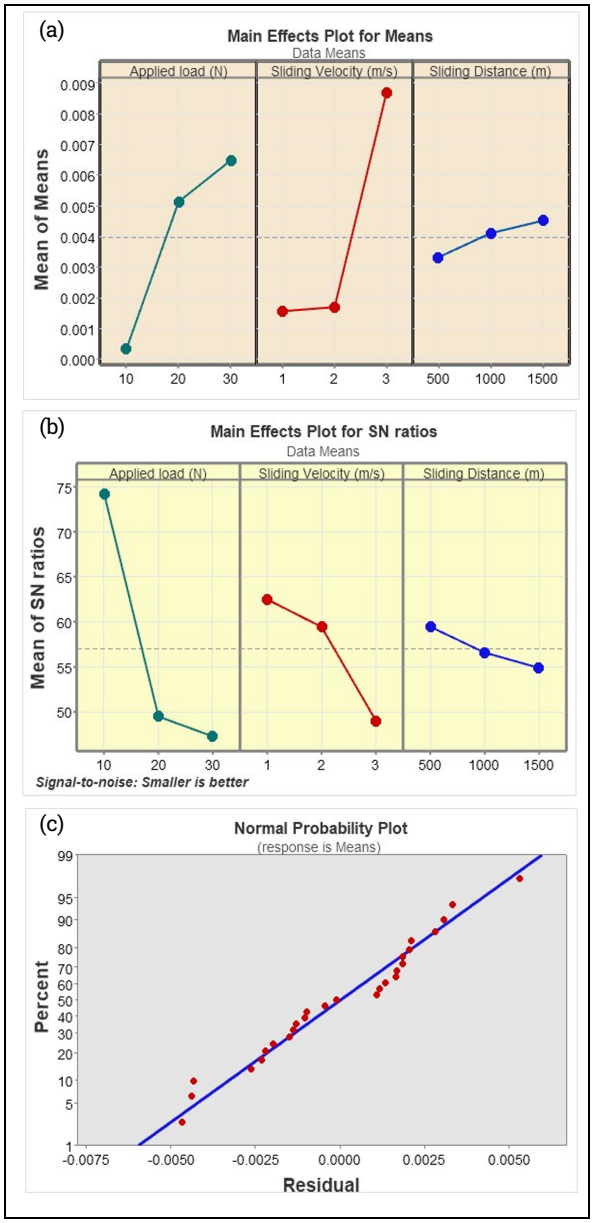


Fig. 5: Main effects plot illustrating the influence of applied load, sliding velocity, and sliding distance on wear rate of WAAM-fabricated Al8090–nano-TiC composite

Table 5. ANOVA for wear rate

Source	DF	Seq SS	Adj SS	Adj MS	F	P
Applied Load (N)	2	0.000188	0.000188	0.000094	11.03	0.001
Sliding Velocity (m/s)	2	0.000298	0.000298	0.000149	17.47	0.000
Sliding Distance (m)	2	0.000007	0.000007	0.000003	0.39	0.085
Residual Error	20	0.000171	0.000171	0.000009		
Total	26	0.000663				

3.3.2 Signal-to-Noise Ratio Analysis for Wear Optimization

The S/N ratio analysis (Fig. 5b) based on the "smaller-is-better" criterion further confirmed the dominance of the applied load and sliding velocity in controlling the wear performance. The response table (Table 6) indicates that the applied load ranked first (Δ = 26.92), followed by the sliding velocity (Δ = 13.53), whereas the sliding distance had the least influence (Δ = 4.56). The highest S/N ratios were observed at lower loads and velocities, indicating improved wear stability under these conditions.

Table 6. Response table for signal to noise ratios of wear rate

Level	Applied Load (N)	Sliding Velocity (m/s)	Sliding Distance (m)
1	74.17	62.49	59.43
2	49.45	59.42	56.57
3	47.25	48.95	54.87
Delta	26.92	13.53	4.56
Rank	1	2	3

This behavior highlights the ability of uniformly dispersed nano-TiC particles to sustain moderate loads by sharing the contact stresses and restricting the matrix deformation. However, at higher loads and velocities, excessive thermal and mechanical stresses overcome the reinforcing effect, resulting in increased wear variability.

3.3.3. Effect of Process Parameters on Coefficient of Friction

The main effects plot for the COF (Fig. 6a) demonstrates a non-monotonic dependence on the applied load and a strong dependence on the sliding velocity. The COF initially increased with the load owing to the increased real contact area and asperity interaction but decreased at higher loads, where the surface conformity improved, and the tribo-oxide layers became more stable. ANOVA confirmed that the applied load significantly influenced the COF ($F = 9.71$, $p = 0.001$), although its effect was secondary to that of the sliding velocity, as listed in Table 7.

Sliding velocity was identified as the most dominant factor governing the COF, with the highest F-value (32.10, $p = 0.000$). At intermediate sliding velocities, a minimum COF was observed, which was attributed to the formation of a compacted tribolayer that reduced the shear resistance. Conversely, at high sliding velocities, the COF increases sharply because of excessive frictional heating, debris accumulation, and unstable sliding conditions. These findings are consistent with the observed transition from mild to

severe wear. The sliding distance had no statistically significant influence on the COF (F = 1.57, p = 0.232), indicating that the frictional behavior was primarily dictated by the instantaneous sliding conditions rather than the cumulative contact duration.

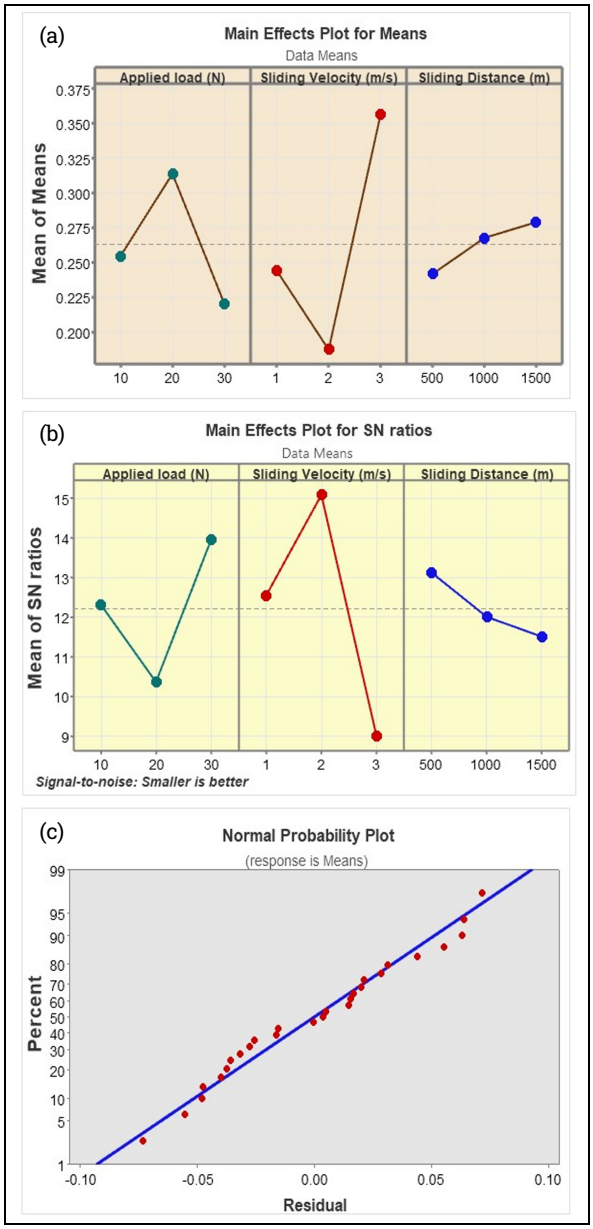


Fig. 6: Main effects plot illustrating the influence of applied load, sliding velocity, and sliding distance on CoF of WAAM-fabricated Al8090–nano-TiC composite

3.3.4 Signal-to-Noise Ratio Analysis for COF

The S/N ratio response table (Table 8) for the COF further substantiates the dominant role of the sliding velocity (Δ = 6.091, Rank 1), followed by the applied load (Δ = 3.595, Rank 2), while the sliding distance remains the least influential factor (Δ = 1.614). The optimal condition for minimizing the COF corresponded to a moderate sliding velocity and load, where the reinforcing effect of nano-TiC and stable tribolayer formation were maximized.

Table 7. ANOVA for CoF

Source	DF	Seq SS	Adj SS	Adj MS	F	P
Applied Load (N)	2	0.040471	0.040471	0.020235	9.71	0.001
Sliding Velocity (m/s)	2	0.133813	0.133813	0.066906	32.10	0.000
Sliding Distance (m)	2	0.006553	0.006553	0.003276	1.57	0.232
Residual Error	20	0.041693	0.041693	0.002085		
Total	26	0.222528				

Table 8. Response table for signal to noise ratios of CoF

Level	Applied load (N)	Sliding Velocity (m/s)	Sliding Distance (m)
1	12.316	12.550	13.121
2	10.361	15.087	12.006
3	13.956	8.996	11.507
Delta	3.595	6.091	1.614
Rank	2	1	3

3.4 Effect of Applied Load on Wear Rate and Coefficient of Friction

The contour plot illustrating the relationship between the applied load, COF, and wear rate, as shown in Fig. 7a, reveals a strong interaction between the contact stress and frictional response. At lower applied loads (10–15 N) combined with low-to-moderate COF values (<0.25), the wear rate remained minimal (<0.003 mm^3/m), indicating a mild wear regime. Under these conditions, the nano-TiC particles effectively shared the applied load, restricted the plastic deformation of the aluminium matrix, and promoted the formation of a stable tribo-oxide layer, thereby minimizing material loss.

As the applied load increased to intermediate levels (20 N), regions of moderate wear (0.003–0.009 mm^3/m) began to appear, particularly at elevated COF values (>0.30). This transition is associated with an increased real contact area and intensified asperity interactions, which lead to micro-ploughing and partial breakdown of the protective tribolayer. At the highest applied load (30 N), localized zones of high wear (>0.012 mm^3/m) were observed at higher COF values, indicating the onset of severe wear. In this regime, subsurface deformation and occasional pull-out of TiC particles contributed to accelerated material removal. The contour analysis confirmed that the applied load is a critical factor governing the wear behavior, particularly when coupled with elevated friction. These

observations are consistent with the ANOVA results, which identified the applied load as a statistically significant contributor to the wear rate variation.

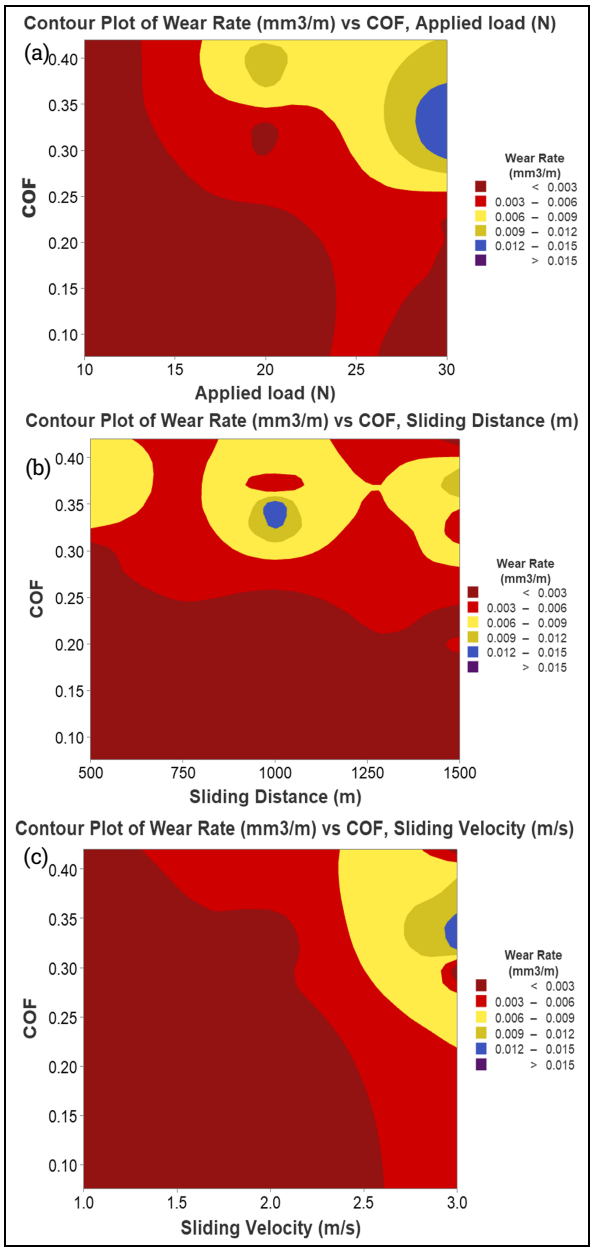


Fig. 7: Contour plots illustrating the interaction effects between coefficient of friction (COF) and (a) applied load, (b) sliding distance and (c) sliding velocity on the wear rate of WAAM-fabricated Al8090–nano-TiC metal matrix composites

3.5 Effect of Sliding Velocity on Wear Rate and Coefficient of Friction

The contour plot representing the sliding velocity versus COF (Fig. 7b) highlights the sliding velocity as the most influential parameter affecting the wear rate. At low to moderate velocities (1–2 m/s) and COF values below 0.25, the wear rate remained low, reflecting stable sliding conditions and limited frictional heating. In this regime, the Al matrix retained sufficient hardness, and the uniformly distributed nano-TiC particles acted as effective load-bearing constituents, thereby suppressing severe material removal. As the sliding velocity increased beyond 2.5 m/s, the contour plot showed a sharp transition to higher wear rates (>0.009 mm^3/m), particularly at elevated COF values. This behavior is primarily attributed to excessive frictional heating, which softens the aluminium matrix and destabilizes the tribo-oxide layer. Under these conditions, TiC particles may detach and act as third-body abrasives, further intensifying wear. The steep gradients observed in the contour plot clearly indicate that the sliding velocity strongly governs the shift from mild to severe wear regimes. The corresponding increase in the COF at high velocities further reinforced the role of unstable sliding and debris accumulation. These findings align well with the ANOVA and signal-to-noise ratio analyses, which ranked the sliding velocity as the dominant parameter influencing both the wear rate and COF.

3.6 Effect of Sliding Distance on Wear Rate and Coefficient of Friction

The contour plot depicting the influence of the sliding distance and COF (Fig. 7c) shows that the sliding distance has a comparatively secondary effect on the wear rate. At lower COF values (<0.25), the wear rate remained low across the entire sliding distance range (500–1500 m), indicating that cumulative sliding did not significantly accelerate wear when stable tribological conditions were maintained. This behavior suggests that the nano-TiC reinforcement and tribolayer formation effectively protected the surface during prolonged sliding. However, at intermediate sliding distances (900–1100 m) combined with higher COF values (>0.30), localized regions of increased wear (0.009–0.015 mm^3/m) were observed. These zones are attributed to tribolayer fatigue and debris accumulation, which temporarily destabilize the contact interface and increase the material loss. At longer sliding distances, wear tends to stabilize, indicating the formation of a compacted debris layer that partially restores surface protection. The COF showed only marginal variation with the sliding distance, confirming that the frictional behavior was primarily controlled by the load and sliding velocity rather than the sliding duration. These observations are consistent with the statistical results, where the sliding distance exhibited the lowest contribution to both the wear rate and COF variation.

3.7 Regression Models for Wear Rate and Coefficient of Friction

To further quantify the relationship between the tribological parameters and performance responses,

multiple linear regression models were developed for the wear rate and COF using the applied load, sliding velocity, and sliding distance as predictor variables. The regression equations provide predictive insights into the relative influence and directionality of each parameter, thereby complementing the statistical and contour analyses.

3.7.1 Regression Model for Wear Rate

The regression equation for the wear rate (Equation 1) indicates that all three process parameters exhibit positive coefficients, confirming that increases in the applied load, sliding velocity, and sliding distance tend to increase the material loss. Among these, the sliding velocity exhibited the largest regression coefficient (0.003557), highlighting its dominant influence on wear behavior. This observation is consistent with the ANOVA and contour plot results, where the sliding velocity was identified as the most significant factor owing to its role in the frictional heating and thermal softening of the aluminium matrix.

Wear Rate (mm^3/m) = -0.01048 + 0.0003075 Applied load (N) + 0.003557 Sliding Velocity (m/s) + 0.00000119 Sliding Distance (m) … (1)

The coefficient associated with the applied load (0.0003075) indicates a moderate increase in the wear rate with increasing normal load, which is attributable to enhanced contact stress and intensified asperity interaction. In contrast, the coefficient for the sliding distance (0.00000119) was comparatively small, confirming its secondary role in governing the wear behavior within the investigated range. This suggests that cumulative sliding contributes marginally to wear once a stable tribolayer is established, which is also observed in the contour plots. The negative intercept in the wear rate equation represents an extrapolated condition and does not have physical significance but indicates that wear becomes appreciable only beyond the threshold combination of load, velocity, and distance.

3.7.2 Regression Model for Coefficient of Friction

The regression equation for the COF (Equation 2) revealed a strong positive dependence on the sliding velocity (0.0562), reaffirming that the velocity-induced thermal effects and debris dynamics dominated the frictional behavior. As the sliding velocity increases, frictional heating promotes instability at the contact interface, resulting in higher COF values. This trend is in excellent agreement with the ANOVA results, where the sliding velocity exhibited the highest F-value and statistical significance. Interestingly, the applied load exhibited a negative coefficient (−0.00173), indicating a slight reduction in the COF with increasing load. This behavior can be attributed to the improved surface conformity and stabilization of the tribo-oxide layers at higher loads, which reduce the interfacial shear resistance. The sliding distance again showed a minimal positive contribution (0.0000372), suggesting that its influence on friction was relatively weak and primarily associated with gradual debris accumulation rather than fundamental changes in contact mechanics.

COF = 0.1478 - 0.00173 Applied load (N) + 0.0562 Sliding Velocity (m/s) + 0.0000372 Sliding Distance (m) … (2)

3.7.3 Consistency with Experimental and Statistical Analyses

The regression coefficients were closely aligned with the trends observed in the main effects plots, S/N ratio analysis, and contour plots, thereby reinforcing the robustness of the developed models. The dominance of the sliding velocity in both regression equations corroborates its ranking as the most influential parameter in the Taguchi analysis, whereas the secondary role of the applied load and minimal influence of the sliding distance are consistent across all analytical approaches.

3.7.4 Predictive Capability and Practical Implications

The developed regression models offer practical utility for predicting the wear rate and COF within the studied parameter domain, enabling the preliminary optimization of operating conditions without exhaustive experimentation. The models indicate that minimizing the sliding velocity and maintaining moderate loads are critical for achieving low wear and stable friction in WAAM-fabricated Al8090–nano-TiC composites. However, caution must be exercised when extrapolating beyond the experimental range, as nonlinear effects, such as severe thermal softening and reinforcement degradation, may become dominant under extreme conditions.

3.8 SEM Analysis of Worn Surface Morphology

The SEM micrograph of the worn surface of the WAAM-fabricated Al8090–nano-TiC composite provides clear evidence of both the successful incorporation of TiC nanoparticles and the evolution of wear mechanisms with increasing applied load (Fig. 8). The SEM image revealed the presence of fine, uniformly distributed bright particulates embedded within the aluminium matrix, attributed to the nano-TiC particles. These particles were well-anchored within the matrix, with no evidence of large agglomerates or interfacial debonding, indicating strong particle–matrix bonding. The absence of extensive particle pull-out cavities further confirms the effective wetting and

metallurgical compatibility between TiC and the Al8090 matrix during WAAM. In addition, the nano-TiC particles appeared to interrupt and deflect wear grooves, demonstrating their role as effective load-bearing constituents. These microstructural features confirm that TiC nanoparticles are not only present but also actively participate in resisting surface deformation, validating their uniform dispersion and functional incorporation within the composite.

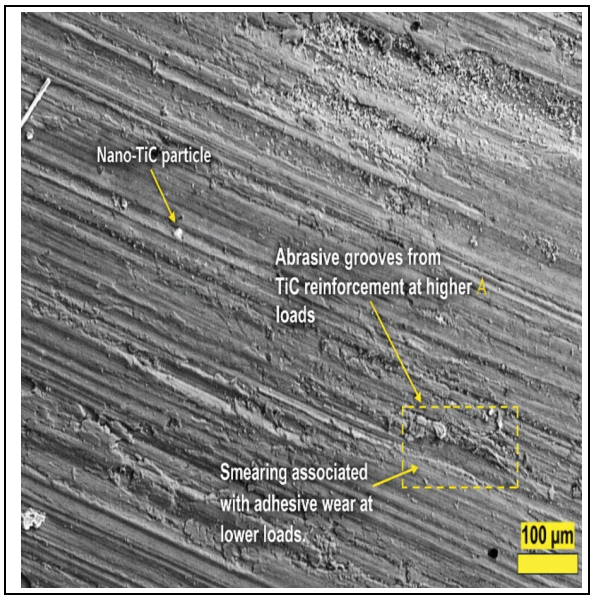


Fig. 8: SEM micrograph of the worn surface of WAAM-fabricated Al8090–nano-TiC composite

At lower applied loads, the worn surface was characterized by shallow parallel grooves aligned with the sliding direction, accompanied by localized surface smearing. These features are indicative of mild adhesive wear, where plastic deformation of the aluminium matrix dominates. The limited groove depth suggests that the nano-TiC particles effectively restricted severe ploughing by supporting part of the applied load and reducing the direct aluminium–counterface contact. The presence of smeared regions further implies localized material transfer and junction formation, which is typical of adhesive wear under mild sliding conditions.

As the applied load increased, the SEM micrographs showed a clear transition in the wear mechanisms. The surface exhibited deeper and more pronounced grooves, along with fragmented debris and micro-cutting marks, which are characteristic of abrasive wear. These features result from increased contact stress and frictional heating, which promote matrix softening and facilitate the abrasive action of hard TiC particles and the detached debris. Localized regions containing compacted wear debris and microcracks suggest the onset of delamination-type fatigue wear under repeated sliding. At higher loads, cyclic subsurface stresses lead to crack initiation and propagation parallel to the surface, eventually resulting in spallation. The coexistence of abrasive grooves and delaminated regions indicates a mixed wear regime, where abrasive and fatigue wear dominate the adhesive mechanisms. The observed transition from adhesive to abrasive fatigue wear with increasing load is consistent with the experimentally measured increase in the wear rate and coefficient of friction. At moderate loads, the uniform dispersion of nano-TiC particles enhanced the load-bearing capacity and stabilized the tribolayer, resulting in lower wear. However, at higher loads, excessive stress and thermal effects overcome the reinforcing benefits, leading to particle pullout, debris formation, and accelerated wear.

4. CONCLUSIONS

This study presents a comprehensive investigation of the tribological performance of WAAM-fabricated Al8090–nano-TiC metal matrix composites, integrating experimental observations with statistical and microstructural analyses. Based on the results obtained, the following conclusions can be drawn.

Successful fabrication of Al8090–nano-TiC composites was achieved using the WAAM process, with SEM and EDS confirming uniform nano-TiC dispersion and strong interfacial bonding within the aluminium matrix. The addition of 1 wt.% nano-TiC significantly improved hardness and load-bearing capacity, with a uniform hardness profile indicating stable WAAM processing. Tribological studies showed that sliding velocity was the dominant factor affecting wear rate and coefficient of friction, followed by applied load, while sliding distance had a lesser influence, as confirmed by Taguchi analysis, ANOVA, contour plots, and regression models. Optimal wear and friction performance occurred at moderate sliding velocity and controlled load, attributed to stable tribolayer formation and effective load sharing by nano-TiC particles. SEM examination of worn surfaces revealed a transition from adhesive wear at lower loads to abrasive and delamination fatigue wear at higher loads and velocities, consistent with wear rate and COF trends. The regression models developed provide a reliable tool for predicting wear and friction behaviour within the investigated range, supporting preliminary process optimization.

4.1 Limitations of the Study

Despite these promising outcomes, the present study has certain limitations. The investigation was confined to a single reinforcement content (1 wt.% nano-TiC) and dry sliding conditions at room temperature. Additionally, the wear behavior was evaluated using a pin-on-disc configuration, which may

not fully represent complex service conditions involving lubrication, impact loading, or elevated temperatures.

4.2 Future Scope and Practical Applications

Future studies should focus on exploring different nano-TiC weight fractions, hybrid reinforcements, and post-deposition heat treatments to further enhance the tribological and mechanical performance. Investigations under lubricated, high-temperature, and corrosive environments, as well as long-term fatigue and impact wear studies, would provide deeper insights into their real-world applicability. From a practical standpoint, the findings of this study demonstrate that WAAM-fabricated Al8090–nano-TiC composites are promising candidates for wear-critical aerospace and automotive components, such as guide rails, sliding brackets, and structural parts subjected to frictional contact, where lightweight designs and enhanced wear resistance are essential.

ACKNOWLEDGEMENTS

The authors gratefully acknowledge the support provided by Sir Issac Newton College of Engineering and Technology for facilitating this research work through access to laboratory facilities, equipment, and technical guidance.

FUNDING

This research received no specific grant from any funding agency in the public, commercial, or not-for-profit sectors.

CONFLICTS OF INTEREST

The authors declare that there is no conflict of interest.

COPYRIGHT

This article is an open-access article distributed under the terms and conditions of the Creative Commons Attribution (CC BY) license (http://creativecommons.org/licenses/by/4.0/).

REFERENCES

Agrawal, J. P., Gupta, N. K. and Somani, N., Effect of TiC particle size on physical, mechanical and tribological properties of Cu-TiC metal matrix composites, *Eng. Res. Exp.,* 5(3), 035009(2023). https://doi.org/10.1088/2631-8695/ACE1D2

Ao, M., Liu, H., Dong, C., Feng, S. and Liu, J., Degradation mechanism of 6063 aluminium matrix composite reinforced with TiC and Al_2O_3 particles, *J. Alloys Compd*., 859, 157838(2021). https://doi.org/10.1016/J.JALLCOM.2020.157838

Arunkumar, S., Ashokkumar, R., Subramani, S. M., Sukethkanna, K. M. and Vigneshwara, S., Optimization of wear behaviour of Al7075 hybrid metal matrix composites using Taguchi approach, *Mater. Today: Proc.,* 33(1),570–577(2020). https://doi.org/10.1016/j.matpr.2020.05.453

Ashok, K. R. and Devaraju, A., Modeling of Mechanical Properties and High Temperature Wear Behavior of Al7075/SiC/CRS Composite Using RSM, *Silicon*, 13, 3499–3519(2021). https://doi.org/10.1007/s12633-020-00801-x

Cabeza, M., Feijoo, I., Merino, P., Pena, G., Perez, M. C., Cruz, S. and Rey, P., Effect of high energy ball milling on the morphology, microstructure and properties of nano-sized TiC particle-reinforced 6005A aluminium alloy matrix composite, *Powder Technol.,* 321, 31–43(2017). https://doi.org/10.1016/J.POWTEC.2017.07.089

Çam, G., Prospects of producing aluminum parts by wire arc additive manufacturing (WAAM), *Mater Today Proc.,* 62, 77–85(2022). https://doi.org/10.1016/J.MATPR.2022.02.137

Chen, J., Han, Y., Li, S., Wei, Z., Le, J., Shi, H., Huang, G., Lu, W. and Di, Z., Evading the strength and ductility trade-off dilemma in titanium matrix composites through designing bimodal grains and micro-nano reinforcements, *Scr Mater*., 235, 115625(2023). https://doi.org/10.1016/J.SCRIPTAMAT.2023.115625

Du, A., Lattanzi, L., Jarfors, A. E. W., Zheng, J., Wang, K. and Yu, G., Role of matrix alloy, reinforcement size and fraction in the sliding wear behaviour of Al-SiCp MMCs against brake pad material, *Wear,* 530–531, 204969(2023). https://doi.org/10.1016/J.WEAR.2023.204969

Dwivedi, S. P., Chaudhary, V. and Sharma, S., Effect of the Addition of Waste Glass Powder along with TiC as Reinforcement on Microstructure, Wettability, Mechanical and Tribological Behavior of AZ91D Magnesium Based Alloy, *Int. J. Metalcasting,* 18(2), 1387-1400(2024). https://doi.org/10.1007/S40962-023-01117-3

Ingarao, G. and Priarone, P. C., A comparative assessment of energy demand and life cycle costs for additive- and subtractive-based manufacturing approaches, *J. Manuf. Process*, 56, 1219–1229(2020). https://doi.org/10.1016/J.JMAPRO.2020.06.009

Kar, C. and Surekha, B., Effect of red mud and TiC on friction and wear characteristics of Al 7075 metal matrix composites, 20, 14-23(2019). https://doi.org/10.1080/14484846.2019.1651138

Karthe, M., Karuppusamy, S., Sureshkumar, B. and Ali, A. N., Mechanical and wear properties of Al7075- B4C–Gr metal matrix composites fabricated by the using stir casting method, *Mater. Today Proc.,* 77, 389–393(2023). https://doi.org/10.1016/J.MATPR.2022.10.162

Kaviyarasan, K., Soundararajan, R., Roger, R. R., Rudresh, S., Ismail, R. S. and Sankar, P. V., Assessing the Tribological Behaviour of Stir Casted AA 6063 with xwt% $ZrSiO_4$ and 6wt% TiB_2 Hybrid Composites, *J. Inst. Eng.,* 103, 85–94(2022). https://doi.org/10.1007/s40033-021-00306-w

Klein, T., Schnall, M., Gomes, B., Piotr, W., Dominik, F. and Morais, P. J., Wire-arc additive manufacturing of a novel high-performance Al-Zn-Mg-Cu alloy: Processing, characterization and feasibility demonstration, *Addit. Manuf*., 37, 101663(2021). https://doi.org/10.1016/J.ADDMA.2020.101663

Le, P. C., Do, T. T., Fang, T. H. and Lee, C. I., Microstructural, interfacial, and frictional properties of TixCy /Ni composites, *Int. J. Mech. Sci.,* 286, 109883(2025). https://doi.org/10.1016/J.IJMECSCI.2024.109883

Li, S. S., Yue, X., Li Q. Y., Peng, H. L., Dong, B. X., Liu, T. S., Yang, H. Y., Jun, F., Shu, S., Feng, Q. and Jiang, Q. C., Development and applications of aluminum alloys for aerospace industry, *J. Mater. Res. Technol.,* 27, 944–983(2023). https://doi.org/10.1016/J.JMRT.2023.09.274

Nouri, S., Sahmani, S., Hadavi, M. and Mirdamadi, S., Mechanical Properties Improvement of Al–Li 8090 Alloy by Using the New Proposed Method of Directional Quenching, *Met. Mater. Int.,* 26(8), 1134–1143(2020). https://doi.org/10.1007/S12540-019-00367-3

Pan, Y., Li, W., Lu, X., Hayat, M. D., Yin, L., Song, W., Qu, X. and Cao, P., Microstructure and tribological properties of titanium matrix composites reinforced with in situ synthesized TiC particles, *Mater. Charact.,* 170, 110633(2020). https://doi.org/10.1016/J.MATCHAR.2020.110633

Qiang, W., Wu, Q. and Long, L., Synergetic softening-strengthening behaviors of gradient nano-grained CoCrFeMnNi high-entropy alloys located in the inverse Hall-Petch range revealed by atomistic simulations, *Int. J. Refract. Metals Hard Mater.,* 123, 106768(2024). https://doi.org/10.1016/J.IJRMHM.2024.106768

Rathod, D. W., A Review on challenges and opportunities in wire arc additive manufacturing of aluminium alloys: Specific context of 7xxx series alloys, *Mech. Eng. Soc. Indus.,* 5(1), 107–124(2025). https://doi.org/10.31603/mesi.12711

Sathish, K., Kumar, S. S., Magal, R. T., Selvaraj, V., Narasimharaj, V., Karthikeyan, R., Sabarinathan, G., Mohit, T. and Kassa, A. E., A Comparative Study on Subtractive Manufacturing and Additive Manufacturing, *Adv. Mater. Sci. Eng.,* 6892641(2022). https://doi.org/10.1155/2022/6892641

Shivakumar, M. R. and Panchangam, M. K., Multi-response optimization of reinforcement parameters of aluminum alloy composites by Taguchi method and grey relational analysis, *Heliyon,* 10(9), e30183(2024). https://doi.org/10.1016/J.HELIYON.2024.E30183

Wang, S. X., Liang, N. N., Wang, B. X., Li, S. F., Misra, R. D. K., Gan, X. M., Zhang, L. and Yang, Y. F., Characterization and orientation-dependent strengthening behavior of intragranular TiC nanoplatelets in titanium matrix composites, Carbon, 233, 119884(2025). https://doi.org/10.1016/J.CARBON.2024.119884

Wang, X. T., Chen, J. H., Kai, M. J., Cheng, L., Hu, Y. Y., Xu, T. R., Wu, S., Zhao, W. L., Song, X. Y., Hu, J. B., Ma, Y. J., Li, G. J. and Cao, Z. H., High friction stress and weak grain-refinement strengthening effect induced by severe lattice distortion in ZrTiNb medium entropy alloys, *Mater. Sci. Eng. A.,* 900, 146522(2024). https://doi.org/10.1016/J.MSEA.2024.146522

Wu, Q. and Pei, N., Effect of SiC concentration on the mechanical properties and fracture modes of SiC/Al composites via cluster analysis of acoustic emission signals*, J. Mech. Sci. Technol.,* 38, 519–526(2024). https://doi.org/10.1007/s12206-024-0102-4

Yekinni, A. A., Bello, S. K., Bajela, G. G. and Adigun, I. A., Effect of Coconut Shell Ash and Graphite Particles on Microstructure and Mechanical Properties of Recycled Aluminium Composites, *Int. J. Adv. Sci. Res. Eng.,* 6(10), 61–71(2020). https://doi.org/10.31695/ijasre.2020.33904

Yu, W., Wang, Y., Li, Y., Qian, X., Wang, H., Chen, Z., Wang, Z. and Xu, G., Texture evolution, segregation behavior, and mechanical properties of 2060 Al-Li (aluminium-lithium) composites reinforced by TiC (titanium carbide) nanoparticles, *Compos. B Eng*., 255, 110611(2023). https://doi.org/10.1016/J.COMPOSITESB.2023.110611

Yu, W., Wang, Y., Li, Y., Wang, H., Chen, Z., Wang, Z. and Xu, G., Texture evolution, segregation behavior, and mechanical properties of 2060 Al-Li (aluminium-lithium) composites reinforced by TiC (titanium carbide) nanoparticles, *Compos. B Eng.,* 255, 110611(2023). https://doi.org/10.1016/J.COMPOSITESB.2023.110611

Zheng, R., Gong, W., Du, J. P., Si, G., Liu, M., Li, G., Takuro, K., Harjo, S., Ma, C., Ogata, S. and Tsuji, N., Rediscovery of Hall-Petch strengthening in bulk ultrafine grained pure Mg at cryogenic temperature: A combined in-situ neutron diffraction and electron microscopy study, *Acta Mater.,* 238, 118243(2022). https://doi.org/10.1016/J.ACTAMAT.2022.118243

Azo Network Site, Aluminum 8090 Alloy (UNS A98090). https://www.azom.com/article.aspx?ArticleID=8789. (2013). Accessed 8 Jan 2026.